Power Consumption Analysis of QKD Networks under Different Protocols and Detector Configurations

Jiaheng Xiong[(1)], Qiaolun Zhang[(1)*], Yoann Piétri[(2)], Raja Yehia[(3)], Raouf Boutaba[(4)], Francesco Musumeci[(1)], Massimo Tornatore[(1)]
[(1)] Politecnico di Milano, Milan, Italy, [(2)] Sorbonne Université, France,
[(3)] Institut de Ciències Fotòniques, Spain, [(4)] University of Waterloo, Canada
Corresponding author: Qiaolun Zhang (qiaolun.zhang@mail.polimi.it)

Abstract

We analyze the power consumption of quantum key distribution (QKD) networks under various protocol and detector configurations. Using realistic network topologies, we evaluate discrete-variable vs continuous-variable QKD and optimize device placement, quantifying power trade-offs of SNSPD vs APD detectors and the benefits of optical bypass.

1 Introduction

As quantum communication networks move toward practical deployment [2], energy efficiency will become a critical concern [5]. QKD enables information-theoretic secure key exchange, but achieving high key rates often requires energy-intensive hardware. In discrete-variable (DV) QKD, detector choice significantly impacts power consumption. For example, *superconducting nanowire single-photon detectors* (SNSPD) offer high detection efficiency, i.e., the probability of registering an incident photon (up to ∼95%), but require cryogenic cooling that consumes thousands of watts [11]. In contrast, avalanche photodiodes (APDs) operate at higher temperatures with lower efficiency (20–30%), but consume far less power as they do not require cryogenic cooling. Prior studies show that SNSPD-based BB84 setups can achieve significantly higher key rates compared to APD-based systems, but this comes at the cost of substantially higher power consumption, highlighting a trade-off between throughput and energy efficiency [11].

We investigate how protocol and detector choices affect network-level energy efficiency under different traffic levels. We study three configurations: (1) CV-QKD with heterodyne detection, (2) BB84 with APDs, and (3) BB84 with SNSPDs. CV-QKD uses balanced photodectors; BB84 relies on single-photon detectors [4]. We evaluate these three configurations across realistic topologies and loads, and under different network architectures (i.e., with and without optical switching), by using a power-aware routing algorithm and a device-level power model, both devised as part of this study.

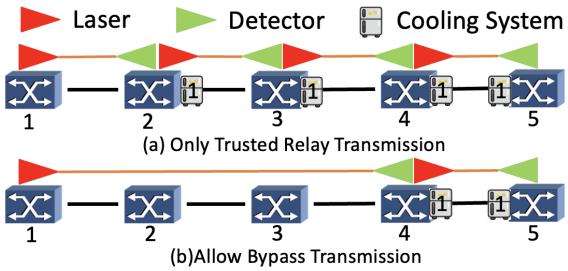

Figure 1. Example of QKD Network Architectures

2 QKD Network Architectures

In a **multi-hop QKD *network***, the way connections are routed can also impact energy consumption. Traditionally, QKD networks use trusted relays at intermediate nodes: each link (hop) generates keys which are then relayed, meaning every hop requires a separate laser and detector as shown in Fig. 1 (a). This architecture (without optical switching) maximizes per-hop key rate by keeping distances short, but it also requires a linearly-increasing number of active lasers and detectors (and thus increases power and equipment cost) at each intermediate node. An alternative is *optical bypassing* [1, 12], wherein intermediate nodes optically switch the quantum signal without measuring it, allowing the end nodes to perform QKD over an end-to-end path as in Fig. 1 (b). This bypass approach reduces the number of active laser-detector (L-D) pairs, potentially saving energy and hardware, at the cost of longer effective link

distances and additional optical loss (e.g., switch insertion loss) [8], which reduces the secret key rate on that path [3].

3 Power Consumption Model of QKD Networks

To compare protocol and hardware energy efficiency, we report the power consumption of each component in Table 1, following the model in Ref. [11]. Note that this work assumes error correction and privacy amplification have the same cost for all protocols as in Ref. [11], and the power consumption might differ if we adopt different assumptions. Each QKD transceiver includes a source (laser transmitter), a detector, and other components such as ADCs, polarization controllers, and TimeTaggers. SNSPD-based detectors require a cooling system, and we assume one cooling system supports up to eight detectors [6]. We attribute all detector power consumption to the shared cooling system and neglect intrinsic per-detector contributions (e.g., biasing and amplifiers), which are negligible compared to the cooling power [9].

The composition of "Other Components" depends on the protocol. In CV-QKD, they include a modulator bias controller, DACs, ADCs, a polarization controller, an optical switch, a local oscillator laser, and two general-purpose computers for hardware control and DSP. In contrast, BB84 systems use motorized wave plates for polarization, an intensity modulator for decoy states, a TimeTagger, and two computers. All these components contribute to the node-level power consumption.

In CV-QKD, DSP energy is characterized by τ_{dsp}, defined as the energy required to process a single symbol. Since τ_{DSP} depends on the specific implementation and processing speed, it is excluded from Table 1. In later sections, we provide indicative DSP power values for various τ_{dsp} to guide implementation.

4 Routing, Wavelength Assignment and Laser-Detector Placement

In QKD networks, the secret key rate between a laser–detector (L–D) pair is fundamentally limited by transmission distance. Due to fiber loss and quantum noise, the key rate decays exponentially with distance, making long-range direct transmission inefficient or infeasible. Thus, the L–D span becomes a key factor in routing decisions and resource consumption.

The resource allocation problem of Routing, Wavelength Assignment, and Laser-Detector Placement (RWALDP) for QKD networks is defined as follows: **Given** a network topology, a traffic matrix, the protocol and L–D type, along with the key rate and power consumption of each device,

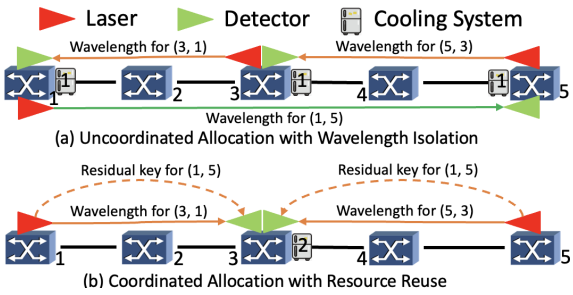

Figure 2. Illustration of Resource Allocation Decisions

determine the wavelength, L–D placement, trusted relay positions, and routing for each request, **subject to** key rate constraints and cooling system capacity (for SNSPDs). The **objective** is to minimize average power consumption.

We demonstrate how optimized resource allocation decisions can reduce network power consumption with two illustrative examples, as shown in Fig. 2. In Fig. 2 (a), each wavelength is exclusively assigned to a single request. Requests (3,1) and (5,3) use the same wavelength but are served independently. Detectors are deployed at Nodes 1 and 3, each requiring its own cooling system. To serve request (1,5), a new wavelength must be allocated, along with a new L–D pair and an additional cooling system at Node 1, resulting in three L–D pairs and three cooling systems in total.

In contrast, Fig. 2 (b) shows a coordinated strategy where different requests can share the same wavelength, and all detectors are colocated at Node 3 using a single cooling system. The key for request (1,5) is generated using the residual key from the existing wavelength between node pairs (1,3) and (5,3), with node 3 acting as the trusted relay. Since no new L–D pair is needed, (1,5) reuses existing infrastructure, reducing the system to two L–D pairs and one cooling system.

To address the RWALDP problem, we propose a multilayer auxiliary graph model to jointly optimize routing, wavelength assignment, and L–D placement in WDM networks. Each layer corresponds to a specific wavelength. For a given traffic demand, candidate wavelength combinations are selected such that their aggregated capacity meets the requirement. Feasible end-to-end paths are then identified, and corresponding L–D placement strategies are evaluated. The model supports resource reuse and accounts for hardware constraints, including the incremental cost of shared cryogenic cooling for colocated single-photon detectors (SNSPDs).

Feasible configurations are abstracted as virtual edges in the auxiliary graph, each annotated with attributes such as selected wavelengths, path sequence, L–D placements, sup-

Table 1. Power consumption of different QKD protocols and hardware components

Power: W	Detector	Source	Detector	Other components	Cooling System
CV-QKD (Gauss)	Heterodyne	2	15	380.45	0
BB84	APD	4	644	912	0
	SNSPD	4	~ 0 (Negligible)	912	3000

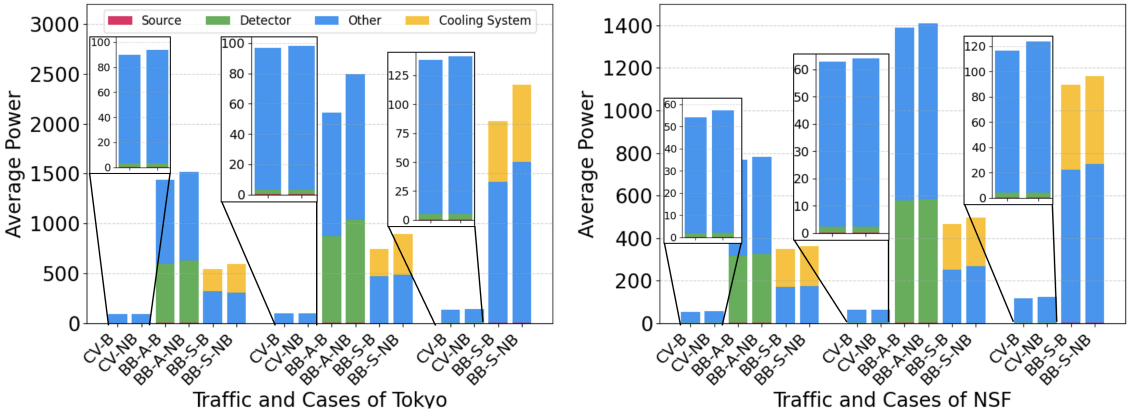

Figure 3. Average power consumption in Tokyo and NSF, $\tau_{dsp} = 10^{-6}$. Each protocol is shown under low, medium, and high traffic loads (left to right). CV = CV-QKD, BB-A = BB84 with APD, BB-S = BB84 with SNSPD; B = with bypass, NB = without bypass.

ported capacity, and estimated power consumption. Edge weights are dynamically computed to reflect power usage, spectrum utilization, traffic-to-key-rate efficiency, and reuse potential. By navigating the auxiliary graph, the algorithm efficiently selects configurations that satisfy key rate and capacity constraints while minimizing power consumption.

5 Numerical Results

We evaluate the power and spectrum usage of QKD networks over two topologies: Tokyo (12 nodes, 21 links) [10] and scaled NSF (23 nodes, 43 links) [7]. Link lengths range from 2.6–12.0 km in Tokyo and 30–130 km in NSF. Each fiber link supports up to 10 wavelengths. Traffic is generated between each pair of nodes, with an average per-pair rate T. For each request, the rate is randomly selected from set $\{T-1000, T, T+1000\}$ bit/s with probabilities of 20%, 60%, and 20%, respectively. We consider three traffic levels: low (50% of maximum network capacity using BB84 with APD), medium (100% of maximum network capacity using BB84 with APD), and high (100% of maximum network capacity using BB84 with SNSPD). CV-QKD (heterodyne) and BB84 with APD or SNSPD are evaluated, each with and without bypass.

Fig. 3 compares the average power consumption of different QKD configurations under three traffic levels in the Tokyo and NSF topologies. CV-QKD configurations (CV-B, CV-NB) consistently exhibit the lowest power, due to both their higher key rates and inherently lower component-level consumption. These results are obtained under the most optimistic DSP efficiency, with $\tau_{dsp} = 10^{-6} J/symbol$ [11]. While a single SNSPD consumes more power than an APD due to cryogenic cooling, BB84 with SNSPD (BB-S) achieves lower network-level power than BB84 with APD (BB-A), thanks to its higher key rate and the ability to share a cooling system among detectors. In all cases, enabling optical bypass (B) reduces overall power compared to trusted-relay-only (NB). In the Tokyo topology, bypass reduces power consumption by up to 20%. In contrast, the reduction in the NSF topology is limited to around 5%, as its longer link distances result in significantly lower provided key rates under bypass, reducing its effectiveness.

Fig. 4 (a) shows that, when τ_{dsp} is high, the DSP dominates total power consumption. In such cases, CV-QKD may consume more power than BB84 with APD or SNSPD, highlighting the importance of efficient DSP design for practical CV-QKD deployment. A value of $\tau_{dsp} = 3 \times 10^{-4}$ was used in the implementation of Ref. [11].

The differences in spectrum occupation are primarily driven by the key rates provided by each configuration. As shown in Fig. 4 (b), we report results only for the Tokyo topology due to space constraints. CV-QKD configurations (CV-B and CV-NB) achieve the lowest spectrum us-

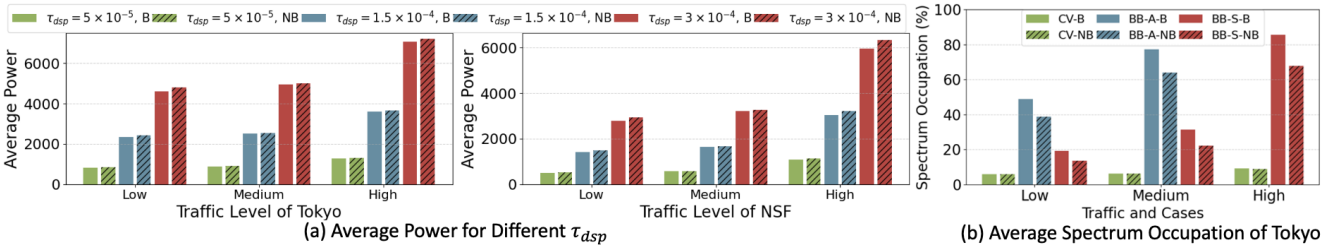

Figure 4. Average Power for Different τ_{dsp} and Average Spectrum Occupation.

age across all traffic levels, while BB84 with APD (BB-A) requires the most. Since lower provided key rates require more parallel wavelengths to meet traffic demands, BB84-APD and BB84-SNSPD consume more spectrum than CV-QKD. Notably, bypass configurations lead to higher spectrum occupation than their no-bypass counterparts in all cases. This is because bypass forces key generation over longer end-to-end links, reducing the achievable key rate and increasing the number of required wavelengths.

6 Conclusions

We presented a power and spectrum usage analysis of QKD networks under different protocol and detector configurations. Results show that CV-QKD achieves the lowest power and spectrum consumption with efficient DSP. BB84 with SNSPD performs better than BB84 with APD at the network level due to higher key rates and shared cooling. Optical bypass reduces power consumption, especially in dense topologies like Tokyo, but may increase spectrum usage. These findings highlight the importance of protocol selection, DSP optimization, and network-aware architecture design for building energy-efficient QKD networks.

This work was supported in part by funding from the Innovation for Defence Excellence and Security (IDEaS) program from the Canadian Department of National Defence (DND).

References

[1] H. H. Brunner, C.-H. F. Fung, M. Peev, R. B. Méndez, L. Ortiz, J. P. Brito, V. Martín, J. M. Rivas-Moscoso, F. Jiménez, A. A. Pastor, et al. Demonstration of a switched cv-qkd network. *EPJ Quantum Technology*, 10(1):38, 2023.

[2] Z. C. Davidson, C. White, A. Sajjad, E. Hugues-Salas, and A. Lord. The quantum age begins: now, 5, 50, or 500 years? an operator perspective on quantum (secure) communication evolution in the next years. In *Next-Generation Optical Communication: Components, Sub-Systems, and Systems XIV*, volume 13374, pages 15–22. SPIE, 2025.

[3] K. Dong, Y. Zhao, X. Yu, A. Nag, and J. Zhang. Auxiliary graph based routing, wavelength, and time-slot assignment in metro quantum optical networks with a novel node structure. *Optics express*, 28(5):5936–5952, 2020.

[4] F. Grosshans, G. Van Assche, J. Wenger, R. Brouri, N. J. Cerf, and P. Grangier. Quantum key distribution using gaussian-modulated coherent states. *Nature*, 421(6920):238–241, 2003.

[5] L. Gyongyosi, S. Imre, and H. V. Nguyen. A survey on quantum channel capacities. *IEEE Communications Surveys & Tutorials*, 20(2):1149–1205, 2018.

[6] Z. Hao, K. Zou, Y. Meng, J.-Y. Yan, F. Li, Y. Huo, C.-Y. Jin, F. Liu, T. Descamps, A. Iovan, et al. High-performance eight-channel system with fractal superconducting nanowire single-photon detectors. *Chip*, 3(2):100087, 2024.

[7] J. Jia, B. Dong, L. Kang, H. Xie, and B. Guo. Cost-optimization-based quantum key distribution over quantum key pool optical networks. *Entropy*, 25(4):661, 2023.

[8] M. Kucharczyk, M. Jachura, M. Jarzyna, K. Banaszek, and A. Ghazisaeidi. Tx-rx mode mismatch effects in gaussian-modulated cv qkd. In *ECOC 2024; 50th European Conference on Optical Communication*, pages 1366–1369. VDE, 2024.

[9] F. Marsili, V. B. Verma, J. A. Stern, S. Harrington, A. E. Lita, T. Gerrits, I. Vayshenker, B. Baek, M. D. Shaw, R. P. Mirin, et al. Detecting single infrared photons with 93% system efficiency. *Nature Photonics*, 7(3):210–214, 2013.

[10] M. Sasaki, M. Fujiwara, H. Ishizuka, W. Klaus, K. Wakui, M. Takeoka, S. Miki, T. Yamashita, Z. Wang, A. Tanaka, et al. Field test of quantum key distribution in the tokyo qkd network. *Optics express*, 19(11):10387–10409, 2011.

[11] R. Yehia, Y. Piétri, C. Pascual-García, P. Lefebvre, and F. Centrone. Energetic analysis of emerging quantum communication protocols. *arXiv preprint arXiv:2410.10661*, 2024.

[12] Q. Zhang, O. Ayoub, A. Gatto, J. Wu, F. Musumeci, and M. Tornatore. Routing, channel, key-rate, and time-slot assignment for qkd in optical networks. *IEEE Transactions on Network and Service Management*, 21(1):148–160, 2023.